Evaluating the Performance of *Jason-2* Open-Loop and Closed-Loop Tracker Modes

CRISTINA MARTIN-PUIG

Global Science and Technology, Inc., at NOAA/Laboratory for Satellite Altimetry, College Park, Maryland

ERIC LEULIETTE AND JOHN LILLIBRIDGE

NOAA/Laboratory for Satellite Altimetry, College Park, Maryland

MÒNICA ROCA

isardSAT LTD, Guildford, Surrey, United Kingdom

(Manuscript received 14 January 2016, in final form 24 May 2016)

ABSTRACT

The Poseidon-3 altimeter on board *Jason-2* includes a significant new capability with respect to its predecessors, an open-loop [Détermination Immédiate d'Orbite par Doris Embarqué (DIODE)/digital elevation model (DEM)] tracker mode. This innovative mode is capable of successfully tracking the backscatter signal over rapidly varying terrains, and thus it overcomes one of the limitations of the closed-loop Poseidon-2 tracker on board *Jason-1*. DIODE/DEM achieves this improvement thanks to a predetermined DEM on board that, when combined with DIODE orbit ephemeris, provides improved acquisition timing and reduced data loss in the coastal zone. As a further enhancement, *Jason-3* and the Sentinel-3 programs will be capable of autonomously switching to this innovative mode in selected regions. To help recommend how these missions should utilize DIODE/DEM, the authors studied the impact of the tracker mode on the accuracy and precision of wave heights and wind speed, the continuity of the sea level climate data record, and the coverage in coastal regions. The results show close agreement between the open- and closed-loop tracker modes over the open ocean with the exception of some differences at high-tidal variability areas, the coastal zone, and sea ice regions. The DIODE/DEM tracker shows better performance than the closed-loop tracker mode at the coast and in the presence of sea ice. *Jason-2*, when operating in open-loop mode, allows for an approximately 5% increase of successful acquisitions at the ocean-to-land transition. However, open-loop tracking exhibits more variability in regions of high tides than closed-loop.

1. Introduction

The Ocean Surface Topography Mission (OSTM) on the *Jason-2* satellite has as its primary goal to extend the data record of ocean surface topography, as well as the derivation of significant wave height and wind speed, beyond its predecessors TOPEX/Poseidon and *Jason-1*. The Poseidon-3 altimeter on board *Jason-2* shares nearly the same architecture as the Poseidon-2 instrument on *Jason-1* (Carayon et al. 2003). This ensures stability across missions, with the addition of a few significant improvements to the tracker. *Jason-1* was designed primarily for ocean observations, and neither its performance near the coast nor over in land or icy regions was optimal (Ablain et al. 2010). To address these limitations, the Poseidon-3 altimeter introduced several tracker upgrades.

The performance of the altimeter relies in part on the success of the tracker on board; it is responsible for tracking and locking the backscatter radar signal within the observation window at a predefined position known as the tracker point. The tracker provides a first guess of range, which after on-ground processing (retracking) is added to the epoch (range window misalignment with respect to the tracker point) and corrected for propagation delays to derive the range to the surface. The tracker has two operational phases: first, it looks for the backscattered signals received by the altimeter (acquisition phase), and second, once the signal is captured its

Corresponding author address: Cristina Martin-Puig, Global Science and Technology, Inc., at Laboratory for Satellite Altimetry, NOAA Center for Weather and Climate Prediction, 5830 University Research Court, College Park, MD 20740.
E-mail: cmpuig@gmail.com

DOI: 10.1175/JTECH-D-16-0011.1

position is locked after compensating for height rate variability and preserving an adequate SNR (tracking phase). The tracker has a predefined incoherent integration time in which 105 echoes are gathered, combined to reduce speckle noise, and processed on board to estimate height displacements and power adjustments for the next acquisition and tracking cycle.

The acquisition phase of Poseidon-2 on *Jason-1* was autonomous and always relied on previous estimates of height and height rate. Its tracking was done with a split-gate algorithm that performed well over the ocean but poorly over nonocean surfaces (Ablain et al. 2010). In the presence of large height variability, or over nonocean surfaces, the tracker would lose track and/or lock, resulting in data loss.

Poseidon-3 on *Jason-2* overcomes these limitations by introducing a new acquisition mode [Détermination Immédiate d'Orbite par Doris Embarqué (DIODE)] and a new tracking algorithm (median); the latter is capable of rapidly adjusting to the surface under observation, and thus it accommodates a wider spectrum of backscattered echoes. However, the proximity to the coastline remains a challenge for conventional trackers (closed loop) and for the first time this satellite also includes a predetermined digital elevation model (DEM) on board, which combined with DIODE provides an accurate initial height estimate. DIODE/DEM, also known as open-loop tracker mode, continues to track over rapidly varying terrain, since it is insensitive to the surface under observation and to the height rate variability. The main purpose of this innovative mode is to improve acquisitions over the coastal zone, inland waters, and sea ice regions without degrading performance over the ocean.

In addition to *Jason-2*, several other current or future missions include an open-loop tracker mode: the Ka-band Altimeter (AltiKa) on *Satellite with Argos Data Collection System (Argos) and AltiKa* (*SARAL*; launched 2013), Sentinel-3A and Sentinel-3B (2016 and 2017, respectively), *Jason-3* (2016), and Sentinel-6/Jason-CS-A and Jason-CS-B (2020). Although theoretically the open-loop mode offers enhanced capabilities over the closed-loop mode, little has been published on its performance (Desjonquères et al. 2010). To assess its use over open ocean and coastal zones, we have conducted the independent study presented in this paper.

Section 2 provides an overview of the different operational tracker modes and their main working phases. Section 3 details the observed impact of each mode on geophysical estimates, through a statistical analysis of the final products. Section 4 directly compares the performance of the open-loop and closed-loop modes. Section 5 discusses issues unique to the DIODE/DEM mode, and section 6 presents our conclusions.

2. Poseidon-3 tracker

Poseidon-3 on *Jason-2* is designed to receive the backscattered echo within an approximately 60-m observation window composed of 128 discrete samples (range bins or gates). To estimate sea level, the tracker must ensure that the radar echo or "waveform" gathered by the altimeter corresponds to the signal bouncing back from the scattering surface, and not to noisy information. When radar returns originate from the open ocean, their returned energy follows a characteristic shape that can be approximated by an analytical function ("the Brown model") (Brown 1977).[1] The leading edge point (LEP) of the echo provides the range measurement and hence sea surface height (SSH). Therefore, the tracker must ensure that the LEP is set within the observation window, close to a predefined range gate known as the tracker point (gate 44 for Poseidon-3). On ground, echoes are fitted to a theoretical model for the derivation of three geophysical estimates: SSH, significant wave height (SWH), and wind speed. For ocean returns from a conventional altimeter, the most common theoretical models are Brown (1977), Hayne (1980), and Amarouche et al. (2004).

a. *Closed-loop upgrades*

1) ACQUISITION PHASE

The objective of acquisition is to correctly initialize the tracker's reception window. This is activated at the beginning of the mission and after a loss of track. The Poseidon-3 altimeter can perform this phase in either autonomous or DIODE mode, in contrast to Poseidon-2 on *Jason-1*, which only supported autonomous acquisition. When acquisition is autonomous, the tracker has no a priori surface or altitude information. The altimetric range guess is made from a test of successive altitude values over a 30-km scanning window. For DIODE acquisition, the range guess is made from a nominal attitude with a range window span of only 5 km. Thanks to this improvement, the acquisition time is reduced from a few seconds ($<$2 s) to approximately half a second, which allows for a reduction in missing measurements (Ablain et al. 2010).

2) TRACKING PHASE

The tracking phase is responsible for positioning the LEP near the tracker point while ensuring an adequate

[1] Figure 1 on page 319 of Thibaut et al. (2010) depicts an open-ocean backscatter waveform shape and the relationship of the waveform to the geophysical variables.

TABLE 1. Poseidon-3 tracker operational configurations.

	Closed-loop mode				Open-loop mode	
	Acquisition		Tracking		Tracking	
Cycle	Auto	DIODE	Split gate	Median	DIODE/DEM, version 2	DIODE/DEM, version 3
0	x		x			
1	x		x	x		
2		x		x		
3		x			x	
4		x		x		
5		x			x	
6		x		x		
7		x			x	
8–33		x		x		
34, 209, 220		x				x
Other		x		x		

SNR (Roca et al. 2009). The Poseidon-3 altimeter has two tracking algorithms available: split gate and median. The first is inherited from Poseidon-2 and relies on adjusting the backscattered echo energy in three range subwindows. *Jason-1* results show that while this algorithm succeeds in tracking oceanlike echoes, it leads to numerous tracking losses for nonocean returns (Ablain et al. 2010). The median tracker has been implemented to correct this weakness and is less sensitive to echo shape. Its principle relies on the cumulative backscatter energy in the whole reception window, which makes it more robust to different echo shapes.

b. Open-loop or DIODE/DEM

The open-loop mode is equivalent to the continuous tracking phase. In this mode the tracker couples the information from the DIODE with an onboard DEM (both referenced to the same geoid). Assuming an ideal DEM, there should be no data loss over any surface. Moreover, an advantage of this mode relies on its insensitivity to the waveform shape. To assess the tracker improvements, a few combinations of acquisition and tracking modes were tested during the commission phase of *Jason-2*. The results demonstrated better performance of the median tracker over split gate, resulting in a ~40% reduction in missing measurements (Ablain et al. 2010). The open-loop mode demonstrated its enhanced capabilities by reducing the data loss to only 3% compared to 10%–15% data loss when the tracker is in closed-loop mode with median tracking. The latter is the operational tracker combination for the *Jason-2* mission. Since commissioning, three complete open-loop cycles have been performed: 34, 209, and 220 (Table 1). These cycles can be used to quantify the performance of open-loop mode versus closed-loop mode.

3. Open-loop geophysical estimate statistics

We compare the statistical results derived from the Sensor Geophysical Data Record, version D (SGDR-D) (Dumont et al. 2015), of each *Jason-2* open-loop cycle with the previous and next cycles, which are both closed loop. We analyze sea surface height anomaly (SSHA), SWH, and backscatter amplitude (σ_0, from which wind speed is derived) at 1 and 20 Hz. The statistical properties measured are mean, standard deviation, median, skewness, and kurtosis.

a. Results at 1 Hz

The 1-Hz data were edited based on ocean surface type, and the 1-Hz quality flag per geophysical quantity (SSHA, SWH, and σ_0) was edited on its own. The nine cycles under analysis (three open-loop cycles with their adjacent closed-loop cycles) show near-perfect agreement between SSHA and σ_0 statistics for open-loop cycles versus closed-loop cycles. However, this is not the case for SWH (Fig. 1). For open-loop cycles, the wave height mean and standard deviation are both ~10 cm smaller than the closed-loop statistics. Kurtosis is ~50% lower in open loop with respect to closed loop, and skewness is in mean ~24% lower (Table 2).

When trying to identify the source of these SWH differences, it was not sufficient to filter SWH with its quality flag. In a least squares estimation of the parameters defining the Brown model, the geophysical retrievals are correlated. The quality flags have different thresholds and thus are sometimes not consistent. Therefore, we decided to filter data if any of the quality flags were set (range, SWH, σ_0). Furthermore, to geographically localize the observations that lead to differences in wave height distribution, we identified a strong link of these contributions with the rain flag and decided to apply it, leading to different findings.

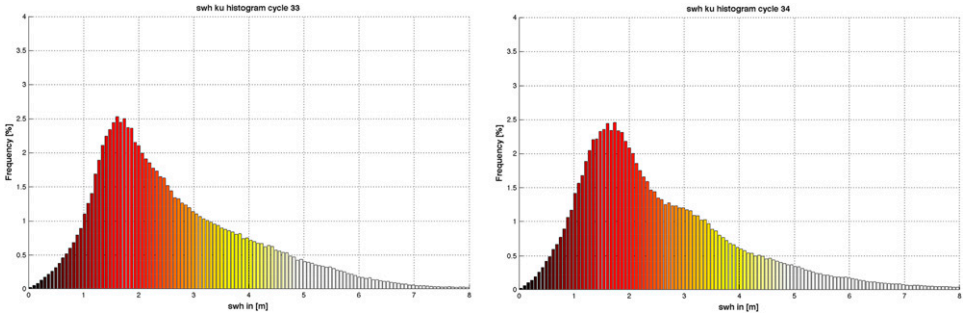

FIG. 1. SWH histograms comparison. (left) Closed-loop cycle vs (right) open-loop cycle. A clear probability distribution function (pdf) shape difference is observed between the histograms with a bump at 3 m due to the coastal contributions in open loop.

Editing all variables based on ocean surface type makes almost no difference in the statistical results, but it highlights one of the expected improvements of the open-loop mode: enhanced acquisition over the coastal region (Fig. 2, top). The analysis confirms that open-loop tracking provides more information in the coastal zone, but these data are edited out by the rain flag (Fig. 2, bottom, which shows that data closer than ~30 km to the coast are rain flagged). If the rain flag is applied, then coastal zone contributions are excluded from the analysis. This naturally leads to an equivalent distribution of wave heights between open- and closed-loop tracking. Therefore, the anomalous statistical behavior of wave height is primarily due to the new coastal contributions.

The rain flag available in the Geophysical Data Records (GDRs) is initiated by first testing three lower-level flags: the altimeter Ku-band backscatter coefficient quality flag (>0 good quality), the flag indicator of the success in the radiometer values to be properly interpolated to the altimeter ground track (>2 successful interpolation), and the radiometer-derived surface time (>0 other than open ocean). If any one of the previous statements is not satisfied, then the rain flag is activated. Otherwise, the rain flag is set when either the liquid water content as measured by the onboard radiometer is higher than a specified threshold ($>0.2\,\mathrm{kg\,m^{-2}}$) or when the difference between the expected and measured Ku-band backscatter coefficients is greater than the rms of the C-band backscatter coefficient (Tournadre and Morland 1997). Because the radiometer-derived sea surface type is mostly set to not-ocean surface at the coast, a revised rain flag will be needed to analyze the DIODE/DEM performance at the coastline.

b. *Results at 20 Hz*

To confirm the 1-Hz findings, we have also processed 20-Hz data. At 20 Hz we have processed epoch (delay time), wave height, and amplitude (σ_0). The results at 20 Hz properly filtered (see previous subsection) confirm the 1-Hz findings for SWH and amplitude. However, 20-Hz data show a wider scattering of the epoch in open-loop cycles compared to closed-loop cycles (Fig. 3) but not in SSHA.

The tracker range, which is added to the epoch to derive SSHA, compensates for the greater scatter in epoch during retracking. The variability in epoch is likely associated with the onboard DEM, and a detailed analysis of the DEM is provided in the appendix. Note that Fig. 3 illustrates epoch stability within the observation window

TABLE 2. The 1-Hz SWH statistics for data edited by the ocean surface type and SWH 1-Hz quality flag. No rain flag filtering has been applied.

Cycle units	Mean (m)	Std dev (m)	Median (m)	Skewness (Ø)	Kurtosis (Ø)
33	2.64	1.57	2.25	2.15	16.70
34	2.54	1.55	2.15	1.63	8.91
35	2.60	1.60	2.19	2.30	17.49
208	2.81	1.55	2.50	2.23	16.01
209	2.74	1.39	2.45	1.61	9.60
210	2.81	1.46	2.53	1.98	16.17
219	2.74	1.73	2.29	2.26	15.62
220	2.65	1.64	2.21	1.60	8.23
221	2.75	1.66	2.35	2.23	16.98

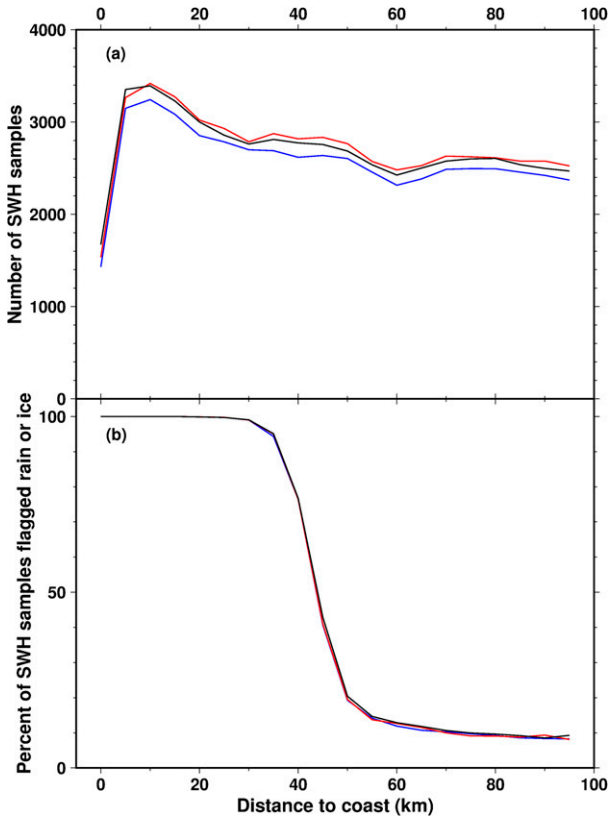

FIG. 2. (top) Number of valid SWH values as a function of distance to the coast in 5-km increments away from the coastal line. DIODE/DEM cycle 34 (black), cycle before 33 (blue), and cycles after 35 (red). (bottom) Percentage of valid SWH values rain flagged as a function of distance to the coast in 5-km increments away from the coastal line, where showing DIODE/DEM cycle 34 (black), cycle before 33 (blue), and cycle after 35 (red).

at 20 Hz, but it does not represent epoch stability of individual echoes within the observation window during tracking—when 95 echoes are incoherently integrated on board to reduce speckle noise and this is repeated every 20 Hz to produce each waveform as provided in the SGDR products. The latter is not desired, since it would lead to blurring associated with height rate changes, yielding undesirable errors in the geophysical retrievals. Height rate blurring is not occurring (N. Picot, CNES, 2014 personal communication).

When plotting the epoch for open-loop cycles, we observe an unforeseen change in epoch (±5 m) at the equator for ascending tracks. This is because each orbital revolution of the DEM is computed separately along track, beginning at the ascending equator crossing. (N. Picot, CNES, 2014, personal communication). This jump is a minor (the pseudo-DEM precision is ±2 m) artifact linked to the way in which the onboard DEM is encoded (Helbert et al. 2007).

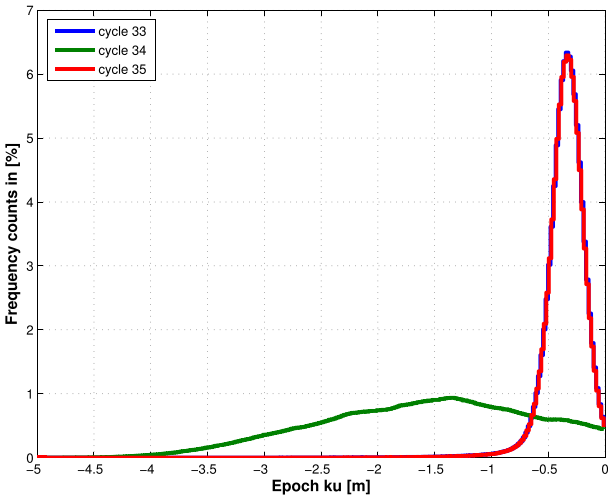

FIG. 3. Example of a 20-Hz Ku-band Epoch pdf. The plot compares the pdf of this retracked variable when the tracker operates in closed-loop mode (cycles 33 and 35) vs open-loop mode (cycle 34). A scatter 4 times larger is observed in open-loop mode compared to closed-loop mode.

4. Tracker modes comparison

The SGDR files always provide a corrected tracker range, as well as a tracker range based on DIODE/DEM. The first is the actual tracker range (either open or closed loop); the second is the tracker range that would be given by DIODE/DEM if the tracker were in open-loop mode, and thus the information is redundant when operating in open loop. The presence of these two values allows us to compare open loop versus closed loop for the entire mission, not limiting us to the three open-loop cycles analyzed in the previous section. The comparison of tracker fields for the closed-loop cycle is of great value to quantify the DIODE/DEM tracker performance. Their comparison for open-loop cycles provides direct verification of the open-loop range values.

To compare the tracker ranges, the 20-Hz DIODE/DEM tracker field needs to be corrected, referenced to the midobservation window, and compensated for height rate variability. The corrections to be applied are the distance between the antenna center of phase and the spacecraft center of gravity (COG), the UltraStable-Oscillator (USO) drift, and the Internal Path Delay correction (IPD). These corrections are all available at 1 Hz in the SGDR. There is also an approximately 9.5-m difference between the tracker ranges due to different referencing within the observation window: beginning and midwindow. The tracker point is at gate 44, while the center of the range window is at gate 64. This difference of 20 gates equates to the ~9.5-m bias.

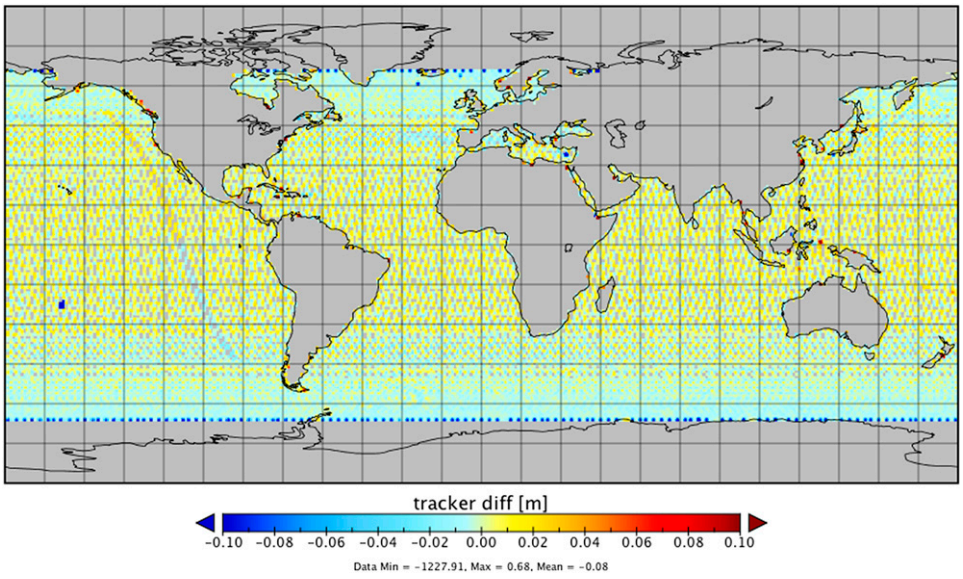

FIG. 4. Gridded map showing the difference in tracker range from open-loop mode and closed-loop mode for the open-loop cycle 34. The differences confirm that both fields correspond to almost identical ranges with a ±2-cm difference among them.

Finally, the DIODE/DEM tracker range needs to be compensated for along-track variations in height rate (h_r). Unfortunately, neither the path delay corrections nor height rate is provided at 20 Hz in the SGDR. Therefore, reproducing the tracker range differences at 20 Hz is not feasible, and the data need to be downsampled to 1 Hz. The tracker range for DIODE/DEM shall be measured by

$$\mathrm{trk_{OL}} = \mathrm{trk_{DIODE/DEM}} - 20\delta_{r.b} + \mathrm{COG} + \mathrm{USO} + \mathrm{IPD} + h_r \mathrm{PRI}(N_p - 1)/2, \quad (1)$$

where $\delta_{r.b}$ is the range bin spacing (for *Jason-2* the bin spacing is 0.468 m or 3.125 ns); PRI stands for pulse repetition interval, which is inversely proportional to the satellite pulse repetition frequency (PRF; ~2 kHz); and N_p is equivalent to the number of incoherently integrated pulses on board (equal to 105, since there are 90 for Ku band and 15 for C band). In open loop, the tracker range differences at 1 Hz are within ±2 cm (Fig. 4). Ideally their difference should be zero, but decimation of the data from 20 to 1 Hz, Eq. (1), introduces a ~2-cm error. This confirms that the tracker ranges from both fields agree for open-loop cycle 34 (Fig. 4).

To compare the operational closed-loop tracker range with its open-loop equivalent, we compute the mean of the difference of the tracker ranges for a full year of data to assess any seasonal effects. *Jason-2* SGDR cycles 35–70 from June 2009 to June 2010 have been processed. Data have been gridded in a 1° × 1° grid using Generic Mapping Tools (UTC; http://gmt.soest.hawaii.edu). The results confirm almost identical performance of open-loop and closed-loop modes over the open ocean, with greater differences seen at the coastal zone and at high latitudes. While the coastal zone results are expected and desired given the nonoptimal performance of the closed-loop mode over the transition from land to ocean, the differences at high latitudes were not anticipated.

Quantification of the mean tracker difference shows it to be approximately ±2 m for most of the ocean, which is equivalent to ±4 range bins or gates, and is an expected result given the resolution of the pseudo-DEM (Helbert et al. 2007). Note this is consistent with the epoch scatter shown in Fig. 3. This is further evidence that retracking compensates for the increased tracker range scattering seen in DIODE/DEM cycles, such that SSHA results remain consistent between the two modes over open ocean. Tracker differences at high latitudes are larger than the epoch scattering, and require further analysis.

To explore the origin of the large differences in tracker ranges at high latitudes, we also need to investigate the seasonal behavior of the differences. Figure 5 illustrates how the differences in tracker fields are correlated with regions of seasonal sea ice. We observe that the closed-loop tracker applies an LEP shift to specular returns (sea ice echoes are largely specular compared to ocean ones). The mean shift is ~16 range bins (about 8 m) as shown in Fig. 6. Epoch differences at the locations of these specular returns should be of the same order, to compensate for this LEP displacement,

and this is confirmed. Therefore, SSHA is again comparable for both open-loop and closed-loop returns in polar regions. One might think of this displacement as a weakness of closed-loop mode versus open-loop mode, but this is not the case. Since specular returns concentrate most of the information in a few range bins around the LEP, a displacement of about 8 m is negligible in its impact to the geophysical estimate. The cause of the displacement is linked in part to the pseudo-DEM on board and is mostly due to the algorithm used for tracking when the altimeter is in close-loop mode. A stable pseudo-DEM cannot accommodate seasonal variability, and thus different LEP of the returned backscatters is expected for open loop at highly variant regions (e.g., sea ice, tides). Median trackers are convenient to deal with a wide variety of scattering returns, in turn convenient for the observation of various types of surface. However, this algorithm positions the median of the waveform at the tracker point with the consequent LEP displacement occurring at surface transition zones, where the backscatter echoes change from oceanlike to specular backscatters (e.g., sea ice leads). The LEP displacement is linked to the different waveform shapes observed for altimetric ocean versus sea ice radar backscatters, with the latter being very specular. The median of an open-ocean waveform is at a greater distance to its LEP than it is for specular returns. Unfortunately, with the limited number of open-loop cycles (two acquired in summer from different years and one acquired in spring), it is not possible to quantify the pseudo-DEM contribution to the observed displacement. Nevertheless, the sea ice height annual variability is within the pseudo-DEM resolution range, and thus a minor contribution is expected.

The variability of the tracker field differences (Fig. 7, top) reveals the sensitivity of the open loop to variations in sea level values, particularly in zones of large tidal variability. Figure 7 (bottom) provides the maximum value of the sum of the geocentric ocean tide, equilibrium and nonequilibrium long-period ocean tide, solid earth tide, load tide, and inverted barometer height corrections during the entire TOPEX/*Jason-1*/*Jason-2* era. The top-to-bottom comparison of Fig. 7's images confirms that the higher the maximum tide, the higher the variations between open-loop and closed-loop tracker ranges. The pseudo-DEM on board is static and does not include real-time tidal predictions.

5. Discussion

While undertaking the activities in section 3, we confronted a known issue in *Jason-2* GDRs: the importance of editing and data flagging, with special attention

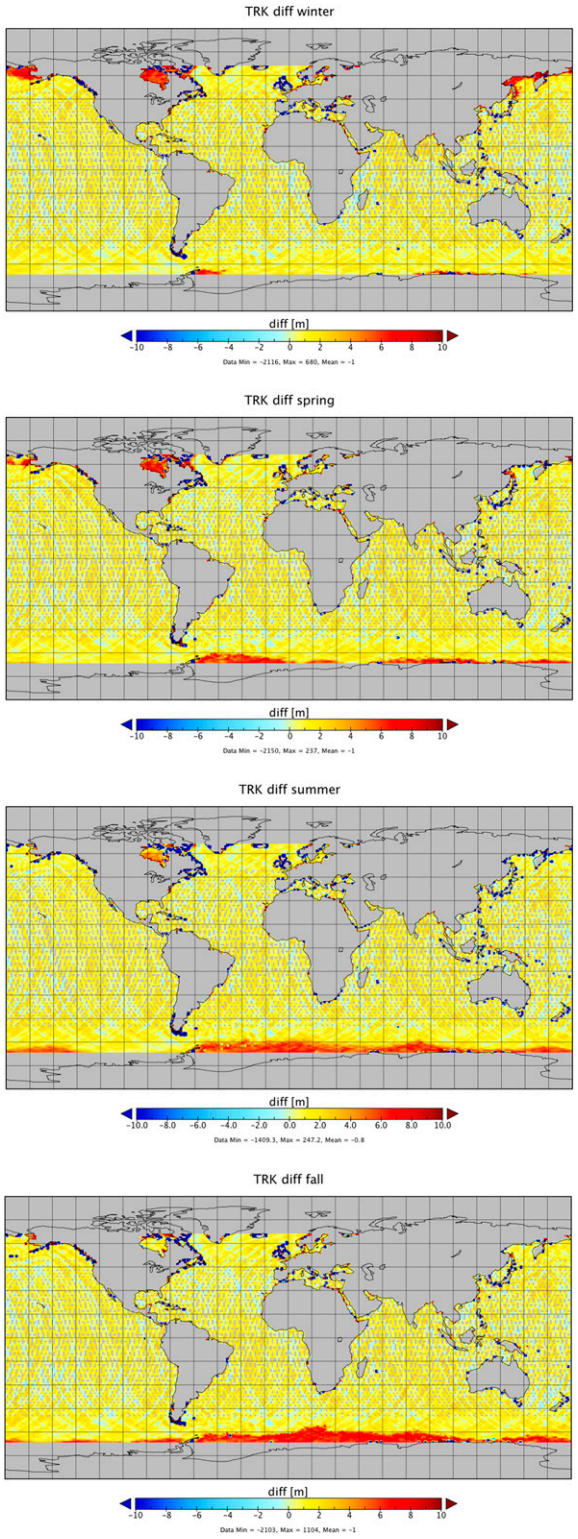

FIG. 5. Seasonal comparison of the mean difference in tracker range from open-loop and closed-loop modes for one year from summer 2009 to summer 2010 split into different seasons. The mean tracker difference observed is 2 m, except for sea ice regions, where differences may be on the order of ±10 m.

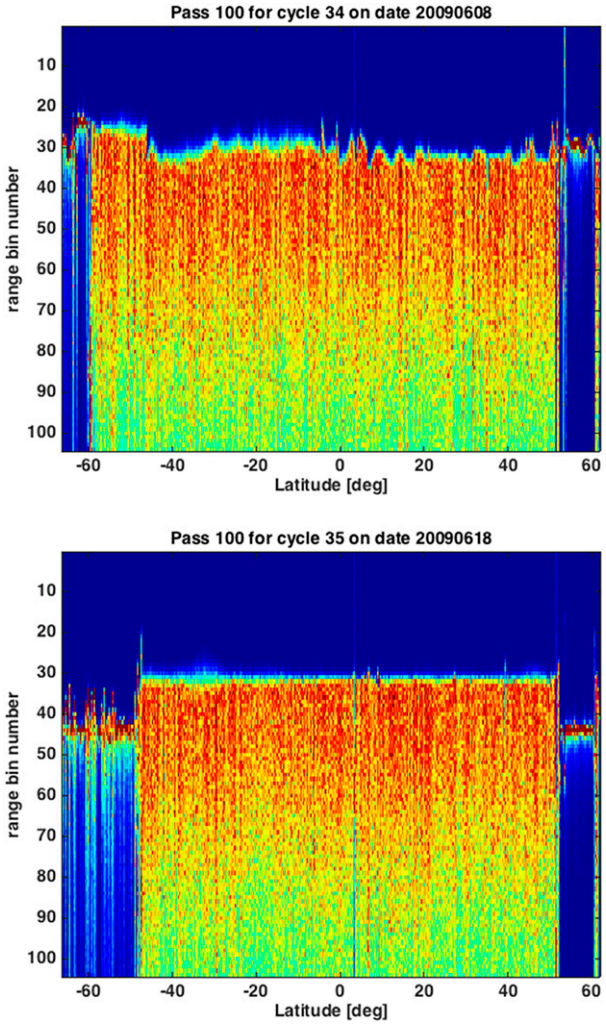

FIG. 6. Ocean surface flagged waveform plot for pass or track 100 in (top) cycle 34 and (bottom) cycle 35, where the tracker operates in different modes. An LEP displacement is clearly depicted in closed-loop (cycle 35) mode of about 16 range bins or 8 m for specular returns (sea ice) vs less displacement with respect to the reference tracker point in open-loop mode (cycle 34). This example shows how DIODE/DEM is capable of preserving the position of the LEP within the observation window at the tracker point for specular backscatters, while this is not the case for closed-loop mode.

paid to the rain flag. The rain flag not only identifies data impacted by rain but also excludes all coastal contributions, and thereby causes a considerable loss of valid data when applied. Our results support revising the edit criteria applied to open-loop observations, to allow for the full exploitation of altimetry data in the coastal zone.

The direct comparison of tracker modes shows that the DEM plays an important role in the accurate positioning of the backscattered echo within the observation window. A quality assessment of the onboard DEM is beyond the scope of this paper, but to support future investigations the appendix provides a detailed description of the steps needed to analyze the pseudo-DEM on board, which at present is not in the public domain.

One of the unique aspects of our analysis is the comparison of the two tracker ranges present in the SGDRs. This has not previously been exploited, and allows us to compare open-loop and closed-loop performance for the entire mission duration, not just the few cycles performed in open-loop mode.

The tracker differences shown in Fig. 6 clearly illustrate that the main differences between open-loop and closed-loop modes occur at high latitudes. The seasonal analysis provided in Fig. 5 shows the correlation of the tracker difference as a function of sea ice coverage. By analyzing one of these regions, the Sea of Okhotsk, we have observed an expected data loss over land while investigating the LEP displacement as discussed in section 4. When this region is covered by ice, data are completely lost when DIODE/DEM is operating as depicted in Fig. 8. Although our work is not land or inland water focused, this result suggests further investigation on the nonocean performance.

With only three cycles of DIODE/DEM data available, it is not possible to provide a detailed regional analysis on the tracker modes' performance. Instead, this is an activity envisioned during the calibration and validation phase of *Jason-3* when both *Jason-2* and 3 will operate in a tandem phase crossing the same location only a minute apart. During this phase every other *Jason-3* cycle will operate in open loop, while *Jason-2* will remain in closed loop (Picot et al. 2015). The tandem phase will allow for direct comparisons of the tracker modes when each satellite observes essentially identical ocean conditions.

Sentinel-3A will operate in synthetic aperture radar (SAR) open-loop mode over the oceans, starting with cycle 2. The mission will operate at higher latitudes than the Jason family and thus allow for a quality assessment of the different operational modes over ice. Note this mission will be sun synchronous, and this has a non-negligible impact on the DEM on board, with special attention given to several corrections (e.g., tides, ionosphere, and wet and dry troposphere path delays) varying diurnally, and thus the use of historical non-sun-synchronous information as depicted in Fig. A2 is no longer valid. Consequently, the pseudo-DEM needs to be adapted for a sun-synchronous mission.

6. Conclusions

For most of the open ocean, we observe close agreement between all 1-Hz geophysical retrievals except for wave height in comparison between open- and

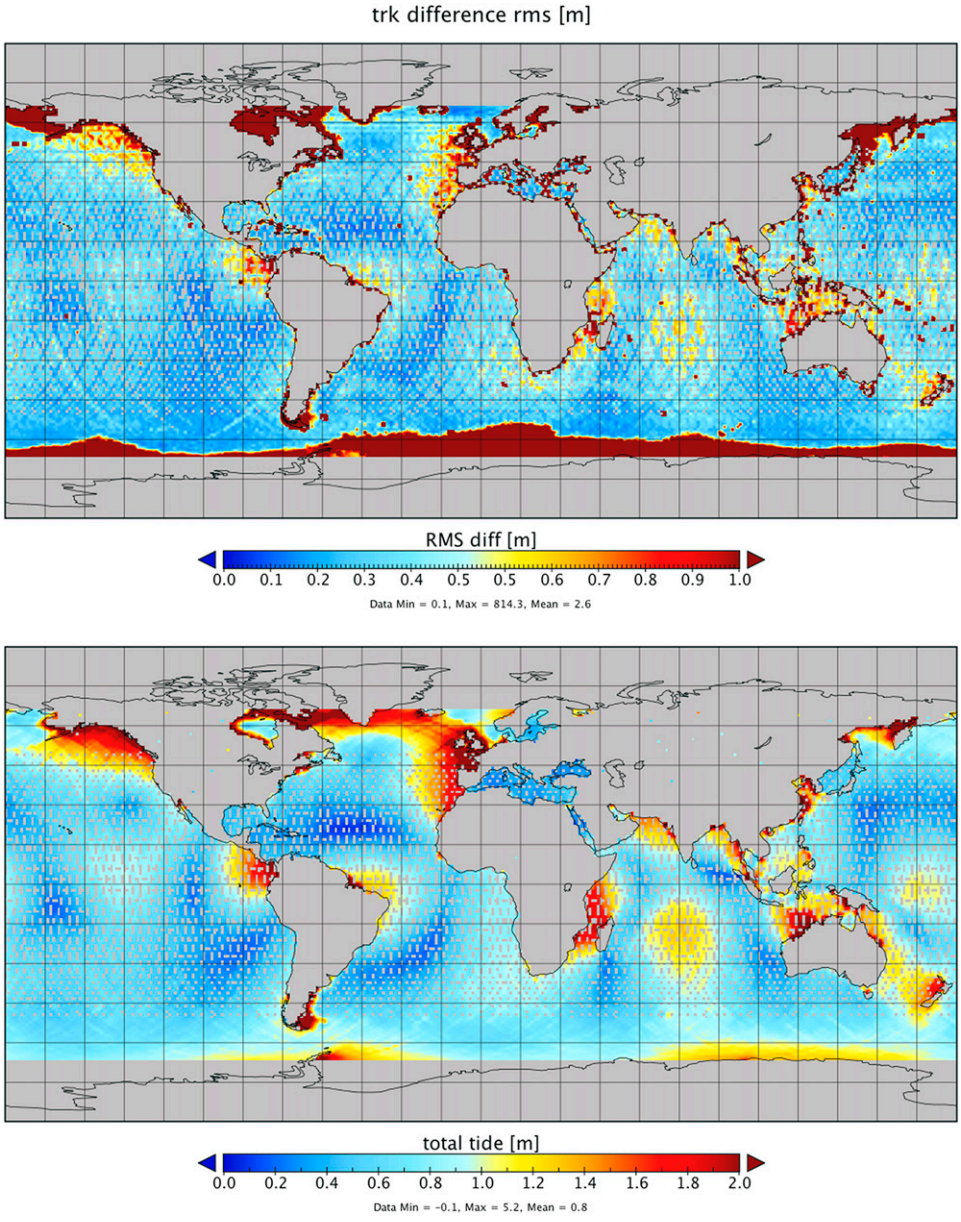

FIG. 7. (top) The rms of tracker differences for one year *Jason-2* mission is compared to (bottom) the amplitude of the maximum total tide during the combined TOPEX–*Jason-1*–*Jason-2* dataset.

closed-loop tracking modes. In the coastal zone, open-loop mode provides more acquisitions, overcoming one of the limitations of the closed-loop mode on *Jason-1*. These new acquisitions at the coastline produce change to the probability distribution function for wave height, which deserves further investigation. However, the coastal observations are edited out by the rain flag as provided in the Geophysical Data Records (GDRs), and our choice was to use the rain flag. Repeating the analysis at 20 Hz confirms the 1-Hz findings and depicts higher variability of the epoch for open-loop mode versus closed-loop mode. This is compensated for during retracking, resulting in no impact to sea level estimates.

Direct comparison of the operational versus DIODE/DEM tracker ranges confirms almost identical performance for most of the ocean except at high latitudes. The mean tracker difference is about 2 m for most of the ocean. Major differences between the trackers are

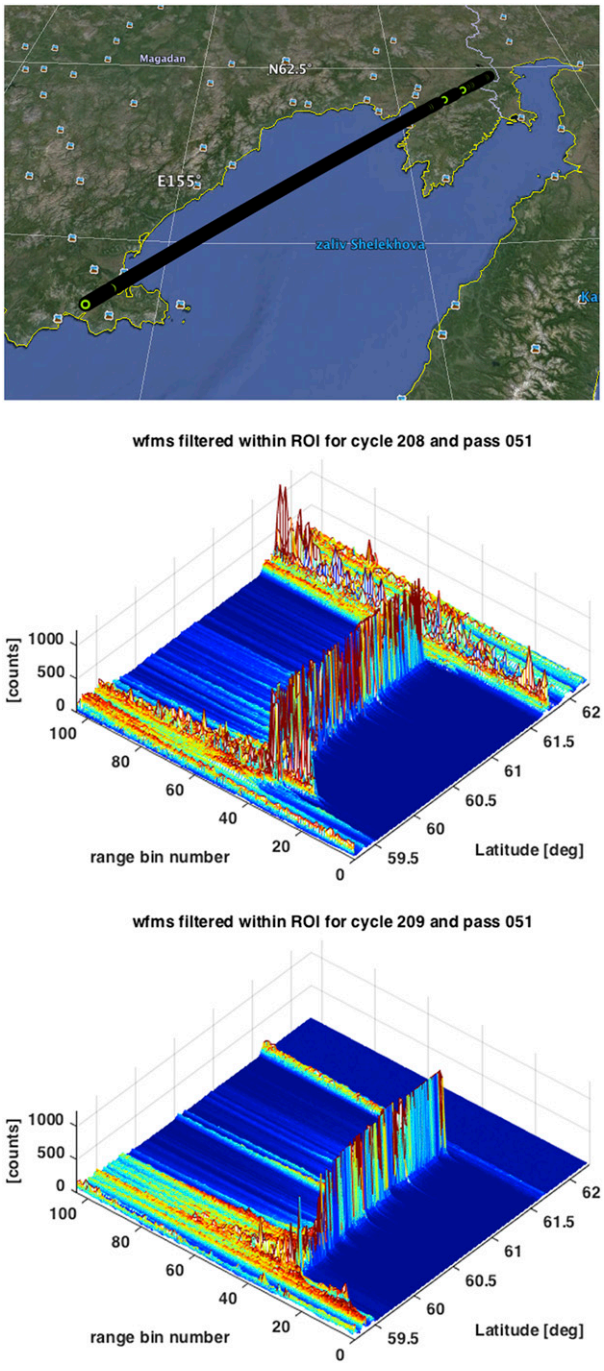

FIG. 8. (top) *Jason-2* pass 51 at the Sea of Okhotsk, (middle) when sea ice is present and clearly shows displacement of the LEP in open-loop mode with respect to reference tracker point (gate 44), and (bottom) a total loss of data over land when this mode is operational.

observed at high latitudes and in areas with large tidal variability. In the presence of high tides, the rms of the tracker range differences shows to be higher but within the *Jason-2* requirements for sea level (1.7-cm rms). Differences between ranges at higher latitudes are in the order of meters (~8 m), which results from the closed-loop median tracking algorithm and its functioning together with the use of an invariant pseudo-DEM that does not assimilate seasonal variability.

Tracker differences observed at high latitudes are primarily linked to the seasonal presence of sea ice. When this occurs the conventional closed-loop tracker introduces a shift in the LEP of about 8 m. Conversely, the open-loop tracker does not introduce such an LEP displacement, and thus the LEP position is more consistent going from open ocean to sea ice. This is neither an advantage nor a disadvantage of one mode versus the other. It is an effect mainly introduced by the median algorithm. A displacement of 8 m has a negligible effect on the quality of the derived geophysical estimates, provided that most of the specular backscatter energy concentrates around its median.

The quality of the pseudo-DEM on board is directly linked with the tracker performance. A quality assessment of this DEM is out of the scope of this paper, but for those interested the pseudo-DEM can be reverse engineered from the operational Geophysical Data Record (OGDR) datasets. An analysis of the pseudo-DEM shows that it is a combination of the CLS01 mean sea surface, corrected for mean values of geophysical propagation corrections, mean tides, and a mean sea state bias.

The motivation of this analysis arose from the need to ensure continuity in the sea level data record. Tracker range and epoch results, from which we derive sea level estimates, confirm that changing the operational tracker mode will not introduce systematic errors into the climate record of sea level or SWH. Moreover, the sea level coastal climate record will be better monitored thanks to the open-loop tracker being capable of operating closer to the coastline.

Acknowledgments. The authors of this paper would like to thank J. D. Desjonquères, F. Boy, and N. Picot from CNES for their collaboration and support in better understanding of the Poseidon-3 tracker on *Jason-2*. This work has been funded by NOAA Grant DOCDG133E10CQ0034. The contents of this manuscript are solely the opinions of the authors and do not constitute a statement of policy, decision, or position on behalf of NOAA or the U.S. government.

APPENDIX

Pseudo-DEM

When operating in DIODE/DEM or open-loop mode, the tracker couples on board the information from the

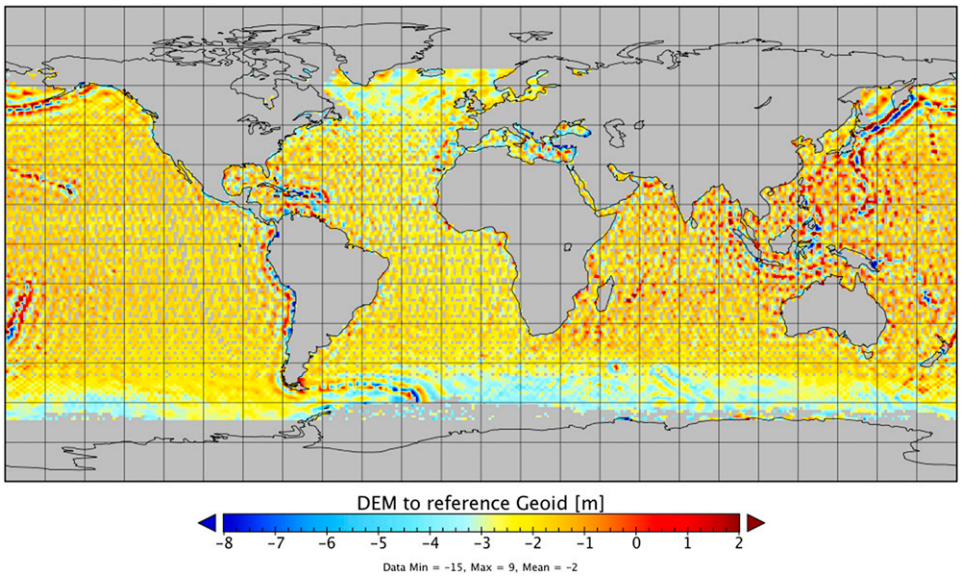

FIG. A1. Pseudo-DEM reverse engineered from *Jason-2* OGDRs with altitude is referenced to the EIGEN-GL04S geoid.

DIODE with a pseudo-DEM. The pseudo-DEM is a compressed version of a DEM derived from the combination of a surface mask and a variety of elevation data files (Desjonquères et al. 2010). The mask was originally derived from the Generic Mapping Tools (UTC), but it has been upgraded at CNES to include missing lakes (Desjonquères et al. 2010). The elevation data result from merging different sources of information per surface type: the CLS01 mean sea surface (MSS) for the ocean (http://www.aviso.altimetry.fr/en/data/products/auxiliary-products/mss.html), the LEGOS Hydroweb database for lakes and rivers (http://www.legos.obs-mip.fr/soa/hydrologie/hydroweb/), and for continental ice shelf the DEM follows Bamber et al. (2001) and Liu et al. (2001).

The onboard pseudo-DEM is a compressed version of the CNES-derived DEM sampled along the *Jason-2* orbit. To fit the DEM into the 1-MB memory space available on board, CNES had to compress the original DEM and exclude some zones. The memory availability for the DEM on *Jason-2* is a limitation still present in *Jason-3*, and it remains a challenge for future missions.

A key component for the open-loop tracker mode quality assessment is the analysis of the pseudo-DEM on board. This is not publicly available, but a close approximation can be derived from OGDRs. These records still preserve the onboard orbit information, thus allowing for the DEM on board to be easily derived from the combination of altitude and range of open-loop cycles (Lambin et al. 2008) as follows:

$$\text{DEM} = \text{ALTITUDE} - \text{RANGE}. \qquad \text{(A1)}$$

However, the difference between altitude and range does not directly provide the pseudo-DEM on board, but it includes instrumental corrections and the reference geoid (EIGEN-GL04S; European Improved Gravity Model of the Earth by New Techniques, version GL04, satellite only). Figure A1 provides the reverse-engineered pseudo-DEM with respect to the reference geoid (Helbert et al. 2007).

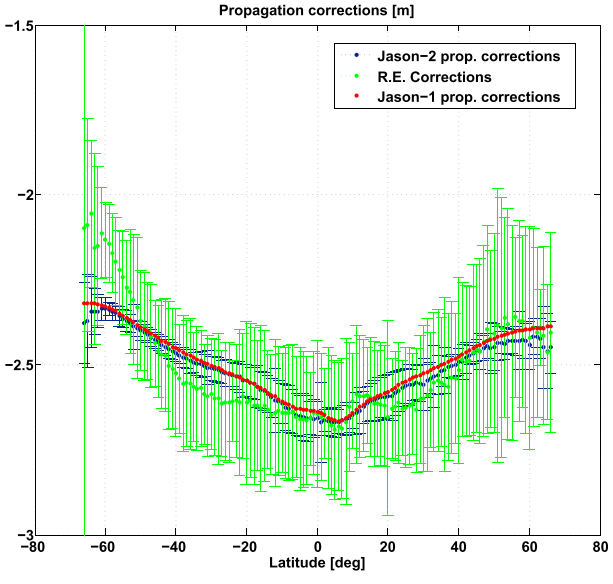

FIG. A2. Propagation corrections as a function of latitude for the combined *Jason-1* and *Jason-2* missions compared to the reverse-engineered propagation corrections.

For verification purposes CNES has provided us the original pseudo-DEM on board in its third version. Differences with respect to the pseudo DEM we derived from the OGDRs are within a few centimeters for most ocean latitudes. Precise global differences in the mean are 9.2 cm with a standard deviation of ~10 cm. Our guess is that the ~9-cm difference observed may be due to the mean sea state bias and the mean global tide, since these may also be added as constants to the DEM. CNES also indicated that the pseudo-DEM, by design, contains mean values of the geophysical corrections (J. D. Desjonqueres, CNES, 2014, personal communication).

Following Desjonquères et al.(2010), the open-ocean contributions to the DEM should be equivalent to the CLS01 mean sea surface. However, after subtracting the MSS from the reverse-engineered pseudo-DEM, we have observed a difference that is constant with latitude coincident with the mean geophysical propagation corrections of the *Jason-1* and *Jason-2* missions as shown in Fig. A2. Therefore, the ocean DEM contribution is not only the CLS01 MSS, but also includes propagation corrections, and it likely includes the mean global sea state bias and mean tides as a global constant.

REFERENCES

Ablain, M., S. Philipps, N. Picot, and E. Bronner, 2010: Jason-2 global statistical assessment and cross-calibration with Jason-1. *Mar. Geod.*, **33** (Suppl.), 162–185, doi:10.1080/01490419.2010.487805.

Amarouche, L., P. Thibaut, O. Zanife, J.-P. Dumont, P. Vincent, and N. Steunou, 2004: Improving the Jason-1 ground retracking to better account for attitude effects. *Mar. Geod.*, **27**, 171–197, doi:10.1080/01490410490465210.

Bamber, J. L., S. Ekholm, and W. Krabill, 2001: A new, high-resolution digital elevation model for Greenland fully validated with airborne laser altimetry data. *J. Geophys. Res.*, **106**, 6733–6745, doi:10.1029/2000JB900365.

Brown, G. S., 1977: The average impulse response of a rough surface and its applications. *IEEE Trans. Antennas Propag.*, **25**, 67–74, doi:10.1109/TAP.1977.1141536.

Carayon, G., N. Steunou, J.-L. Courrière, and P. Thibaut, 2003: Poseidon-2 radar altimeter design and results of in-flight performances. *Mar. Geod.*, **26**, 159–165, doi:10.1080/714044516.

Desjonquères, J., G. Carayon, N. Steunou, and J. Lambin, 2010: Poseidon-3 radar altimeter: New modes and in-flight performances. *Mar. Geod.*, **33** (Suppl.), 57–79, doi:10.1080/01490419.2010.488970.

Dumont, J., and Coauthors, 2015: OSTM/Jason-2 products handbook. Tech. Rep., Version 1.9, CNES SALP-MU-M-OP-15815-CN, EUMETSAT EUM/OPS-JAS/MAN/08/0041, JPL OSTM-29-1237, NOAA/NESDIS Polar Series/OSTM J400, 65 pp. [Available online at http://www.aviso.altimetry.fr/fileadmin/documents/data/tools/hdbk_j2.pdf.]

Hayne, G. S., 1980: Radar altimeter mean return waveforms from near-normal-incidence ocean surface scattering. *IEEE Trans. Antennas Propag.*, **28**, 687–692, doi:10.1109/TAP.1980.1142398.

Helbert, J., and Coauthors, 2007: Generation of DEMs for the new tracking mode using DIODE real-time navigator information onboard Poseidon-3 and AltiKa. [Available online at http://www.aviso.altimetry.fr/fileadmin/documents/OSTST/2007/helbert.pdf.]

Lambin, J., J.-D. Desjonquères, N. Steunou, and J. Helbert, 2008: OSTM/Jason-2 and AltiKa new tracking modes. [Available online at http://cioss.coas.oregonstate.edu/CIOSS/workshops/Altimeter_workshop_08/Coastal_Alt_Presentations/21_Lambin_Jason-2_Tracking_Modes.pdf.]

Liu, H., K. Jezek, B. Li, and Z. Zhao, 2001: Radarsat Antarctic Mapping Project digital elevation model, version 2. NASA National Snow and Ice Data Center Distributed Active Archive Center, accessed 24 May 2016. [Available online at http://nsidc.org/data/nsidc-0082.]

Picot, N., A. Guillot, S. Desai, B. Haines, H. Bonekamp, R. Scharroo, J. Lillibridge, and E. Leuliette, 2015: Jason-3 calval plan. Tech. Rep. TP4-J0-PLS-1158-CNES, 68 pp.

Roca, M., S. Laxon, and C. Zeli, 2009: The EnviSat-RA2 instrument design and tracking performance. *IEEE Trans. Geosci. Remote Sens.*, **47**, 3489–3506, doi:10.1109/TGRS.2009.2020793.

Thibaut, P., J. Poisson, E. Bronner, and N. Picot, 2010: Relative performance of the MLE3 and MLE4 retracking algorithms on Jason-2 altimeter waveforms. *Mar. Geod.*, **33** (Suppl.), 317–335, doi:10.1080/01490419.2010.491033.

Tournadre, J., and J. Morland, 1997: The effects of rain on TOPEX/Poseidon altimeter data. *IEEE Trans. Geosci. Remote Sens.*, **35**, 1117–1135, doi:10.1109/36.628780.